

Electronic Supporting Information for

Surface polymerization of melamine resin on a perovskite: enhancing the efficiency and stability of solar cells

Tianyu Li, Yuyan Zhang, Lingyi Fang, Bing Zhang, Yi Yuan, Jing Zhang and Peng Wang*

State Key Laboratory of Silicon and Advanced Semiconductor Materials, Department of Chemistry, Zhejiang University, Hangzhou 310030, China

*Corresponding author.

E-mail address: pw2015@zju.edu.cn (P. Wang).

1. Experimental section

1.1. Materials

Acetone ($\geq 99.5\%$, Sinopharm Chemical Reagent), ethanol (99.7%, Aladdin), titanium diisopropoxide bis(acetylacetonate) (TIACA, 75% in isopropanol, Sigma-Aldrich), acetylacetone (ACAC, $> 99.0\%$, TCI), TiO₂ paste (30NR-D, Greatcell Solar), SnO₂ colloid precursor (15% in H₂O colloidal dispersion, Alfa Aesar), lead iodide (PbI₂, 99.99%, TCI), lead bromide (PbBr₂, 99.99%, TCI), formamidinium iodide (FAI, 99.0%, Greatcell Solar), methylammonium bromide (MABr, 99.0%, Greatcell Solar), CsI (99.0%, TCI), rubidium chloride (RbCl, 99.9%, 3A Chemicals), methylammonium chloride (MACl, $\geq 99.5\%$, Xi'an Polymer Light Technology Corp.), dimethyl sulfoxide (DMSO, 99.9%, Sigma-Aldrich), *N,N*-dimethylformamide (DMF, 99.8%, Sigma-Aldrich), zinc iodide (ZnI₂, 99.995%, Alfa Aesar), hexakis(methoxymethyl)melamine (HMMM, 98%, TCI), isopropyl alcohol (IPA, $> 99.8\%$, Sigma-Aldrich), 4-*tert*-butylpyridine (TBP, 96%, Sigma-Aldrich), polystyrene (PS, Sigma-Aldrich), [6,6]-phenyl-C61-butyric acid methyl ester (PCBM, 99%, Sigma-Aldrich), poly(3,4-ethylenedioxythiophene) polystyrene sulfonate (PEDOT:PSS, 1.3–1.7% solution in water, Xi'an Polymer Light Technology), and chlorobenzene (99.8%, Sigma-Aldrich) were purchased from commercial resources and used as received without further purification. TBTA[6]H and 4-*tert*-butylpyridinium bis(trifluoromethanesulfonyl)imide (TBPHTFSI) were prepared according to the literature methods.^{1,2}

1.2. General instrumentation

Attenuated total reflection-Fourier transform infrared (ATR-FTIR) spectra were acquired using a Vertex 70 FTIR spectrometer (Bruker). Ultraviolet-visible (UV-vis) absorption spectra were measured with a Cary 8454 spectrophotometer (Agilent). Steady-state photoluminescence (PL) spectra and time-resolved PL (TRPL) decays were obtained using a Life-Spec-II fluorescence spectrometer (Edinburgh), with excitation wavelengths of 475 nm or 375 nm. X-ray photoelectron spectra (XPS) were measured using an ESCALAB 250Xi instrument (Thermo Scientific) with a monochromatic Al K α X-ray source (1486.6 eV). The binding energy scale was referenced to the C 1s signal. X-ray diffraction (XRD) patterns of thin films were collected with a SmartLab diffractometer (Rigaku) using Cu K α radiation ($\lambda = 0.15418$ nm) operated at 7200 W power (40 kV, 180 mA). Top-view surface morphologies were imaged using an SU70 field emission scanning electron microscope (Hitachi). Fluorescence optical microscope (FOM) images were captured on an ECLIPSE Ti-U system (Nikon).

1.3. Perovskite samples on glass for photoluminescence measurement

A 1.2-mm thick glass slide (25 mm \times 16 mm) was cleaned sequentially with detergent, deionized water, acetone, and ethanol in an ultrasonic bath for 10 min. The precursor solution for perovskite was prepared by adding 1.30 M of PbI₂, 0.14 M of PbBr₂, 1.19 M of FAI, 0.14 M of MABr, and 0.07 M of CsI to a mixture of DMSO and DMF (*v/v*, 1/4). The precursor solution was deposited onto the glass substrate using a consecutive two-step spin-coating process at 1000 rpm for 10 s (ramp rate 200 rpm s⁻¹) and 6000 rpm for 30 s (ramp rate 2000 rpm s⁻¹). At 15 s before the end of the program, 150 μ L of chlorobenzene was added onto the spinning substrate. The film was annealed at 120 °C for 1 h to form the CsMAFA based perovskite film. Subsequently, 50 μ L of IPA solution of ZnI₂ (4 mg mL⁻¹) was dropped onto the top of the perovskite film, which was then spin-coated at 3000 rpm for 30 s. The film was annealed at

80 °C in the dark for 10 min to produce PbI₂-modified perovskite.³ For the melamine-formaldehyde resin (MF) modified film, 50 μL of IPA solution of HMMM (2 mg mL⁻¹) was spin-coated onto the perovskite layer at 3000 rpm for 30 s. The film was annealed at 80 °C for 30 min. Next, a PS solution of 20 mg mL⁻¹ in chlorobenzene was spin-coated atop the perovskite films with and without MF at 5000 rpm for 30 s. Finally, a ~100 nm-thick gold layer was thermally evaporated under a vacuum of $\leq 1 \times 10^{-4}$ Pa. The samples were covered with waterproof adhesive tape and further sealed with an epoxy adhesive (3M).

1.4. Modeling of HMMM dimer absorbed on perovskite

To model the CsMAFA perovskite film, we performed DFT calculations using FAPbI₃ as a model system due to the abundance of formamidinium cations and iodide anions. The calculations were carried out using the ADF BAND package at the GGA:revPBE-D3/DZ level, with a $4 \times 4 \times 3$ FAPbI₃ perovskite slab oriented along the 110 direction. Geometry optimization was performed using a plane-wave basis with an energy cutoff of 400 eV and an energy convergence threshold of 1.0×10^{-5} eV. The charge density difference plot between HMMM dimer and FAPbI₃ was calculated using a Monkhorst-Pack k-point mesh of $2 \times 1 \times 1$.

1.5. Fabrication, encapsulation, and disassembly of CsMAFA based solar cells

Pre-cleaned fluorine-doped tin oxide (FTO) glass was used as the substrate for the deposition of a compact TiO₂ (c-TiO₂) layer by spray pyrolysis using an ethanolic solution of TIACA and ACAC. A mesoporous TiO₂ (m-TiO₂) layer, approximately 200 nm thick, was spin-coated onto the c-TiO₂ layer using an ethanolic solution of TiO₂ colloid formulated with commercial 30NR-D TiO₂ paste. The resulting film was sintered at 450 °C to produce the TiO₂-coated FTO electrode. The perovskite layer was deposited onto the TiO₂ electrode following the same protocol described in section 1.3. The HTL was spin-coated at 5000 rpm for 30 s using a chlorobenzene solution formulated with 35 mg mL⁻¹ of TBTA[6]H, 6.18 mg mL⁻¹ of TBPHTFSI, and 132 mM TBP. The gold electrode (~80 nm) was deposited using a shadow mask under a vacuum of $\leq 1 \times 10^{-4}$ Pa. The device was kept in dry air (< 2% RH) overnight, covered with waterproof adhesive tape, and further sealed with epoxy adhesive (3M). The active area of the cells used in this study is approximately 0.5×0.5 cm². For fundamental characterizations, the sealing materials, gold electrode, and HTL were removed if necessary.

1.6. Fabrication of FAPbI₃ based solar cells

An indium tin oxide (ITO) glass substrate ($12 \Omega \text{ sq}^{-1}$) was laser-etched and underwent meticulous cleaning by sequential rinsing with detergent, deionized water, acetone, and IPA for 10 minutes in an ultrasonic bath. A thin layer of SnO₂ nanoparticles (3%, diluted in water) was deposited onto the ITO glass by spin-coating at 3000 rpm for 30 s. The coated substrate was then annealed in ambient air at 150 °C for 30 min and subjected to UV-ozone treatment. The glass/ITO/SnO₂ substrates were transferred into a glove box filled with dry air for perovskite film deposition. A two-step spin-coating method was used to fabricate the perovskite layer. First, a solution containing 1.5 M PbI₂ and 7.5 mM RbCl in a DMSO:DMF solvent mixture (*v/v*, 1/9) was spin-coated onto the SnO₂ layer at 1500 rpm for 30 s, followed by annealing at 70 °C for 1 min. Once the PbI₂ layer had cooled to room temperature, a mixture solution of FAI:MAcI (90 mg:13.5 mg in 1 mL IPA) was spin-coated onto the PbI₂ layer at 1800 rpm for 30 s. The resulting film was then annealed at 150 °C for 30 min to form the FAPbI₃ perovskite layer,

which contained a small amount of $(\text{PbI}_2)_2\text{RbCl}$.⁴ For the MF-modified solar cell, 50 μL IPA solution of HMMM (2 mg mL^{-1}) was spin-coated onto the perovskite layer at 3000 rpm for 30 s, followed by annealing at 110 $^\circ\text{C}$ for 30 min. An HTL was then deposited using a chlorobenzene solution containing 50 mg mL^{-1} of TBTA[6]H, 8.8 mg mL^{-1} of TBPHTFSI, and 132 mM of TBP, at a spin-coating speed of 5000 rpm. Finally, an 80 nm thick gold electrode was deposited on top of the HTL using thermal evaporation under a vacuum of less than 10^{-4} Pa. The device was kept in dry air (< 2% RH) overnight and covered with a waterproof adhesive tape.

1.7. Photocurrent–voltage and external quantum efficiency measurements

The photocurrent density–voltage (J – V) characteristics were measured by applying a bias potential to the testing cell and recording the photocurrent using a Keithley 2400 source meter under full computer control, with measurements fully automated using Labview 14.0. To provide 100 mW cm^{-2} of AM 1.5G sunlight, an LS1000-4S-AM solar simulator (Solar Light Company) was used, and the light intensity was calibrated using a monocrystalline silicon solar cell (Model HG-SS20, No. L0013, Beijing Henggong Instrument Co. Ltd., China). External quantum efficiency (EQE) curves were obtained by measuring the photocurrent with a Keithley 2400 source meter and an Omni- λ 300 monochromator (Zolix, China) equipped with a 150 W xenon lamp (Zolix, China). The wavelength sampling interval was 10 nm, and the current sampling time was 1 s, with measurements fully automated under computer control. The EQE measurement was calibrated using a Hamamatsu S1337-1010BQ silicon diode at the National Institute of Metrology, China. A black mask with an aperture area of 0.16 cm^2 was placed on the testing cell during all measurements, and the experiments were conducted in a dry air-filled glove box.

1.8. Trap density and mobility measurements

For the electron-only device, we used the same FTO, TiO_2 , and perovskite layers as in PSCs. A chlorobenzene solution of PCBM (20 mg mL^{-1}) was spin-coated onto the top of the perovskite layer at 2000 rpm for 30 s. Finally, an 80 nm-thick silver electrode was thermally evaporated in high vacuum ($\leq 1 \times 10^{-4}$ Pa). For the hole-only device, we first deposited a 40 nm-thick layer of PEDOT:PSS on top of ITO glass. Onto the PEDOT:PSS layer, we deposited the CsMAFA perovskite layer and the TBTA[6]H-based HTL layer in turn. Finally, an 80 nm-thick gold layer was thermally evaporated. Dark current–voltage (I – V) curves were measured in the range of 0 to 2.5 V using a Keithley 2400 source meter. The logarithmic plot of the dark I – V curve was divided into three regions, including the ohmic region in the low-bias region, the trap-filled-limited (TFL) region, and the space-charge-limited current (SCLC) region in the high-bias region. From the linear fittings in the ohmic and TFL regions, we derived the TFL voltage (V_{TFL}), which is related to the density of trap states (n_t) by equation 1,

$$n_t = \frac{2\varepsilon_0\varepsilon_r V_{\text{TFL}}}{eL^2}, \quad (1)$$

where ε_0 and ε_r respectively refer to the vacuum and relative permittivities of the perovskite, e is the elementary charge, and L refers to the thickness of the corresponding perovskite films. We derived the electron or hole mobility ($\mu_{e,h}$) of the perovskite by fitting the $J^{1/2}$ – V curves in the SCLC regions using the Mott-Gurney law,

$$J = \frac{9}{8} \varepsilon_0 \varepsilon_r \mu_{e,h} \frac{V^2}{L^3}. \quad (2)$$

1.9. Impedance and capacitance–voltage measurements

Impedance spectra measurements were conducted using an Autolab PGSTAT302N electrochemical workstation, employing a small perturbation of 20 mV across a wide frequency range spanning from 10 Hz to 3 MHz. To obtain capacitance–frequency spectra of the solar cells, we corrected the real and imaginary parts of the measured impedance to exclude the influences of series resistance (R_s) and parasitic inductance (L_i), which exhibit dominance at higher frequencies. The calculation of capacitance (C) involved the utilization of equation 3,

$$C = -\frac{1}{\omega} \left[\frac{Z'' - \omega L_i}{(Z' - R_s)^2 + (Z'' - \omega L_i)^2} \right], \quad (3)$$

where Z' and Z'' denote the real and imaginary parts of impedance, respectively, and ω represents the angular frequency. By systematically measuring the capacitance (C) at varying bias potentials (V) and plotting C^{-2} as a function of V , we gained insights into the interrelationship between the two variables. Furthermore, we derived the interfacial charge density (N) and the built-in voltage (V_{bi}) of the PSCs by fitting the acquired Mott-Schottky plots to equation 4,

$$C^{-2} = \frac{2}{A^2 e \varepsilon_0 \varepsilon_r N} (V_{bi} - V), \quad (4)$$

where A corresponds to the area of the solar cell, e symbolizes the elementary charge, and ε_0 and ε_r respectively denote the vacuum and relative permittivities of the perovskite material.

1.10. Thermostability and operational stability tests

To evaluate the thermostability of the sealed PSCs and dummy cells, we exposed them to a high-temperature environment using an FD56 oven (Binder, Germany) set at 85 °C, with the relative humidity in our lab ranging from 40–90%. At regular intervals, we removed the cells from the oven to perform J – V measurements under the AM 1.5G conditions. To assess the operational stability of the PSCs, we conducted maximum power point (MPP) tracking measurements at 65 °C under continuous illumination from an SLS-LED-80A solar simulator. To minimize any potential environmental interference, we placed the cells inside a nitrogen-filled glovebox during the measurements. We utilized the standard perturb and observe method to collect the MPP data at five-minute intervals.

2. References

- 1 N. Xu, Y. Zhang, L. Fang, T. Li, X. Xie, J. Zhang and P. Wang, *ACS Mater. Lett.*, 2022, **4**, 11.
- 2 Y. Ren, M. Ren, X. Xie, J. Wang, Y. Cai, Y. Yuan, J. Zhang and P. Wang, *Nano Energy*, 2021, **81**, 105655.
- 3 T. Li, M. Ren, Y. Zhang, L. Fang, J. Zhang, Y. Yuan, J. Zhang and P. Wang, *Small*, 2020, **16**, 2001866.
- 4 Y. Zhao, F. Ma, Z. Qu, S. Yu, T. Shen, H.-X. Deng, X. Chu, X. Peng, Y. Yuan, X. Zhang and J. You, *Science*, 2022, **377**, 531.

3. Additional data

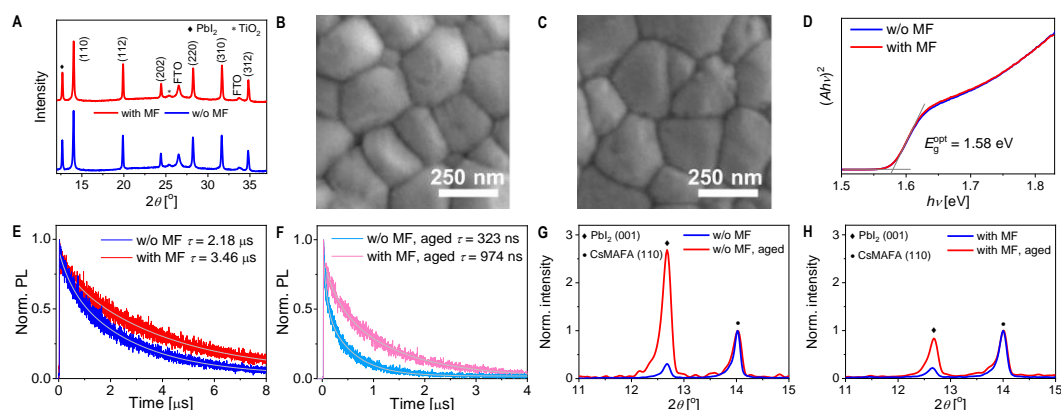


Fig. S1 (A) X-ray diffraction (XRD) patterns of the CsMAFA perovskite films with and without melamine formaldehyde (MF) modification. The perovskite films are deposited on the mesoporous TiO₂ coated FTO glass. The peak observed at $2\theta = 14.0^\circ$ corresponds to the diffraction of the (110) plane of the α -phase perovskite. The intensities of other diffraction peaks are normalized based on this peak intensity. The presence of the PbI₂ (001) diffraction at $2\theta = 12.7^\circ$ is attributed to the addition of a slight excess of lead iodide to the perovskite precursor solution. (B and C) Top-view scanning electron microscope images of the perovskite films (B) without and (C) with MF. (D) Tauc plots of the perovskite films with and without MF, showing the corresponding optical bandgaps (E_g^{opt}). (E) Time-resolved photoluminescence (PL) traces of perovskite films with and without MF. The gray lines are biexponential decay fits. (F) Time-resolved PL traces of 2,000 h, 85 °C aged perovskite films with and without MF. The gray lines are biexponential decay fits. (G) XRD patterns of perovskite films before and after 2,000 h, 85 °C aging. (H) XRD patterns of MF-modified perovskite films before and after thermal aging.

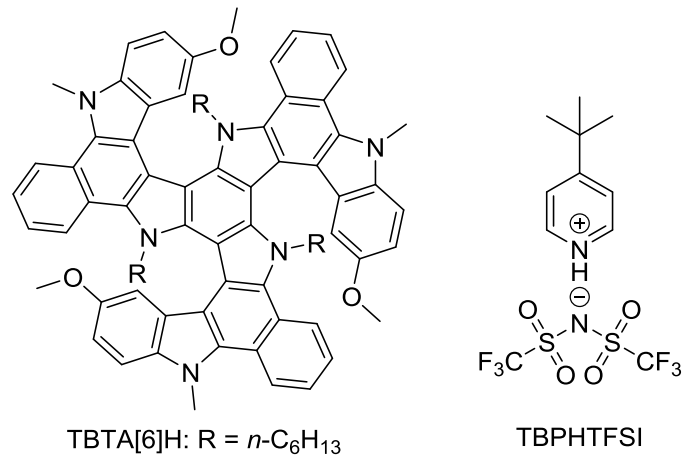


Fig. S2 Molecular structures of molecular semiconductor TBTA[6]H and air-doping promoter TBPHTFSI.

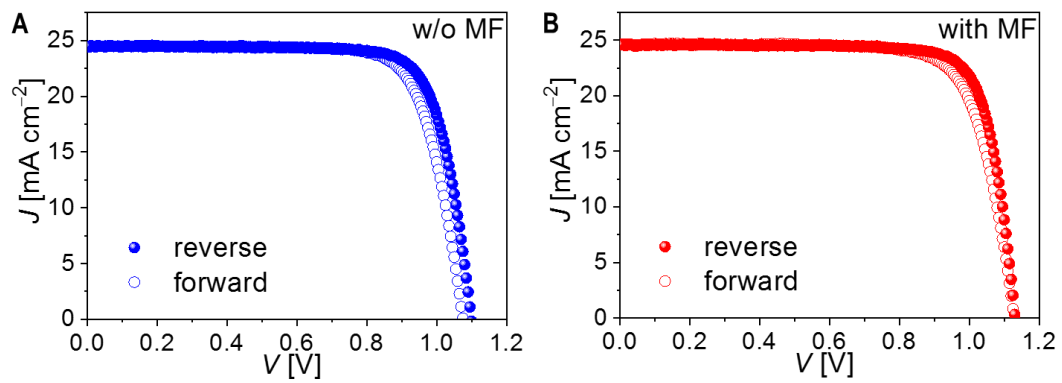


Fig. S3 Forward and reverse scan J - V curves of typical perovskite solar cells (A) without and (B) with MF, under the simulated AM 1.5G irradiation.

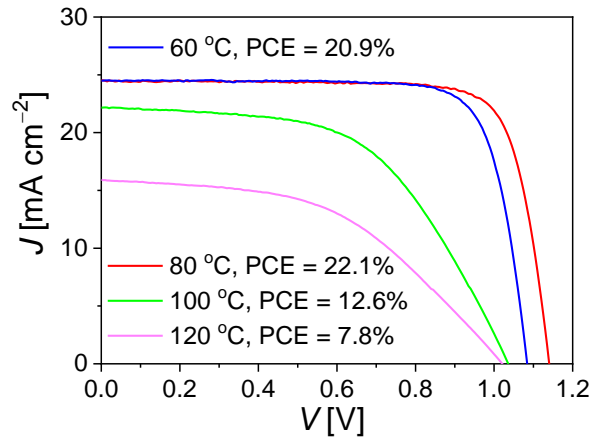


Fig. S4 Representative photocurrent density–voltage (J – V) curves of perovskite solar cells with MF layer polymerized at varying temperatures.

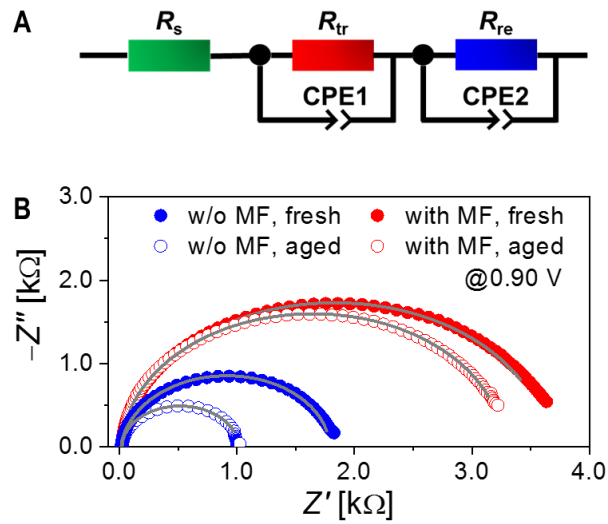


Fig. S5 (A) An equivalent circuit used to fit impedance spectra. (B) Nyquist plots at a bias potential of 0.90 V.

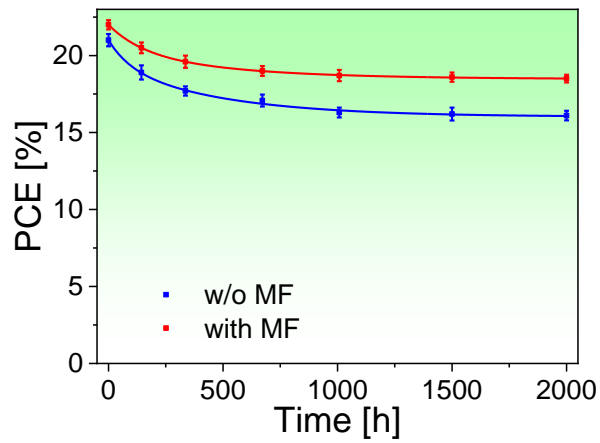


Fig. S6 Temporal evolution of power conversion efficiency (PCE) of solar cells. The aging was conducted at 85 °C.

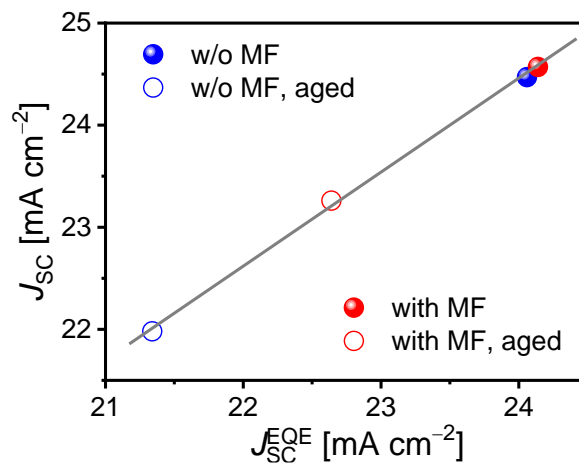


Fig. S7 Relation between J_{SC} and J_{SC}^{EQE} .

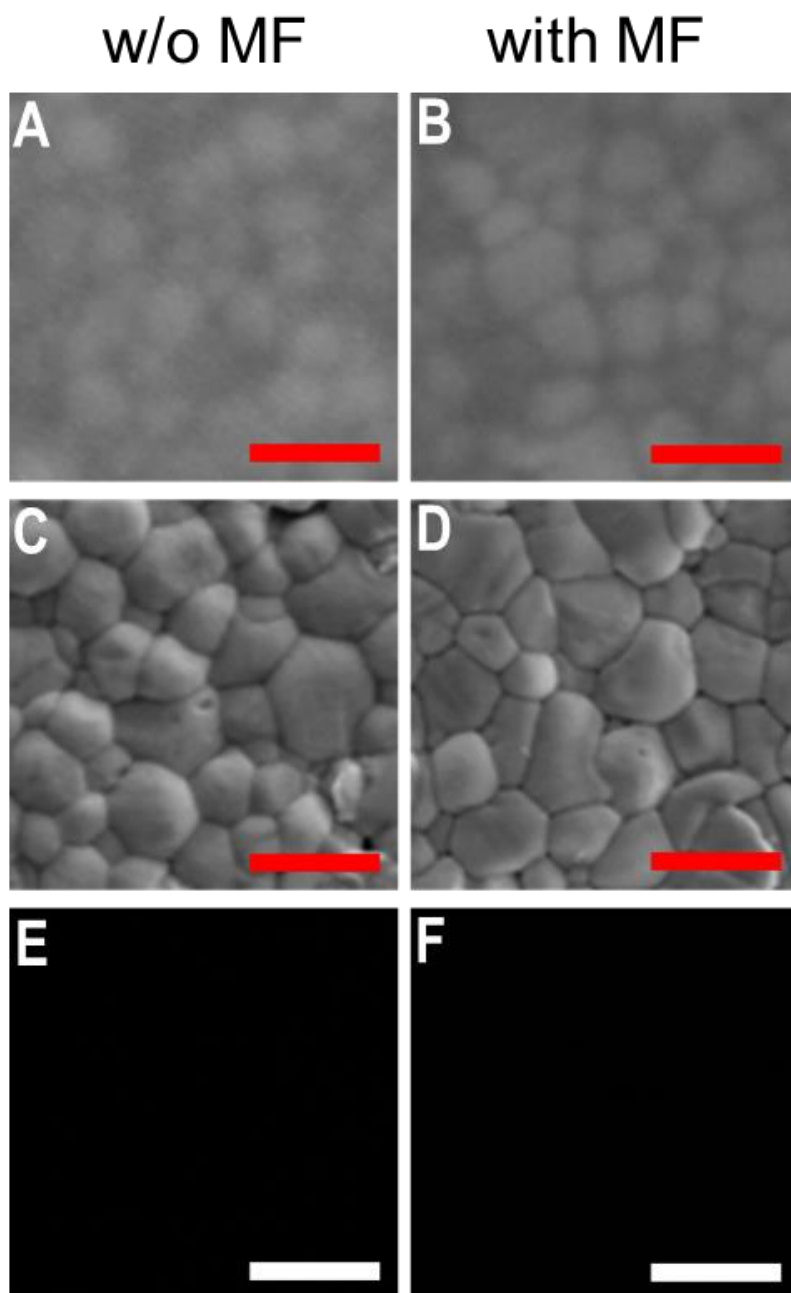


Fig. S8 (A and B) Top-view scanning electron microscope (SEM) images of the HTL in the perovskite solar cells prior to aging: (A) w/o MF; (B) with MF. The gold layer were removed prior to imaging. Scale bar: 500 nm. (C and D) Top-view SEM images of the perovskite layer in the perovskite solar cells prior to aging: (C) w/o MF; (D) with MF. The hole transport layer was removed using chlorobenzene prior to imaging. Scale bar: 500 nm. (E and F) Fluorescence optical microscope images of the perovskite layer in the solar cells prior to aging: (E) w/o MF; (F) with MF.

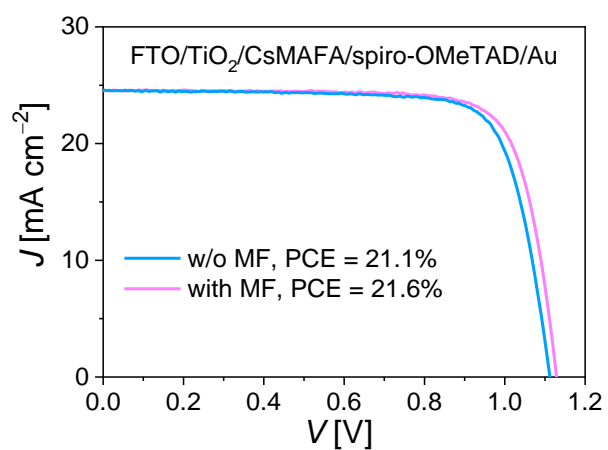


Fig. S9 Typical photocurrent density–voltage (J – V) curves of the spiro-OMeTAD based perovskite solar cell under the simulated AM 1.5G irradiation.